ACS OMEGA

http://pubs.acs.org/journal/acsodf

Article

Hydrodynamic Modeling of Turbulence Modulation by Particles in a Swirling Gas−Particle Two-Phase Flow

Yang Liu,* Lixiang Jiang, and Yongju Zhang

Cite This: *ACS Omega* 2021, 6, 10106−10118

Read Online

ACCESS | Metrics & More | Article Recommendations | Supporting Information

ABSTRACT: Turbulence modulations by particles of a swirling gas−particle two-phase flow in an axisymmetric chamber are numerically simulated. To fully consider the preferential concentrations and the anisotropic dispersions of particles, a second-order moment model coupling particle−particle collision model was improved. Experimental validation for the proposed model, algorithm, and in-house codes by acceptable match was carried out. The effects of ultralight-expanded graphite and heavy copper particles with a large span of Stokes number on gas velocities and fluctuations, Reynolds shear stresses and tensor invariants, turbulence kinetic energies, and vortice structures are investigated. The results show that turbulent modulation exhibits strong anisotropic characteristics and remains in a close relationship with the flow structure. Modulation disturbances and vortex evolution are enforced by heavy-large particles with higher Stokes numbers. Preferential accumulations of ultralight particles in shear stress regions at lower vortices are weaker than those of heavy particles. For axial turbulence modulations, a heavy particle plays the primary role in the inhibition action because of larger inertia, and a light particle contributes to the enhancement effect due to excellent followability. The instantaneous flow information and coherent turbulent structure are failed to be acquired due to the limitation of the Reynolds time-averaged algorithm.

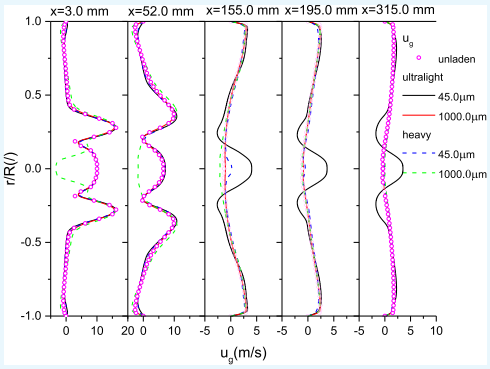

INTRODUCTION

A swirling gas−particle flow exists in all kinds of natural phenomena and industrial processes, such as the coal combustion, the circulated fluidized bed, the chemical process, and the environment protection, and so forth. Gas turbulence plays an important role in the transfer of mass, momentum, and energy between gas and particle phases. It is very indispensable to obtain further understanding regarding the flow mechanism and turbulence modification by effects of particle properties, particle dispersion, and turbulent flow structure.[1−5]

Experimental investigations via the particle image velocity (PIV), laser Doppler anemometry (LDA), a phase Doppler particle analyzer (PDPA), and a high-speed camera have been successfully performed for the hydrodynamic gas−particle turbulent flows.[6−17] As for the LDA technique, interactions between small-dense copper and glass beads with diameters of 70, 50, and 90 μm and gas turbulence behaviors in a fully developed channel were measured. Particles could respond to some specific scales of turbulent motion, and gas turbulence was attenuated by the addition of particles.[6] Gas turbulence modulation in the streamwise direction reaches up to approximately 35% decrease along the channel-flow extension regions.[7] Turbulence intensity was significantly changed in the higher particle concentration regions, and the turbulence intensity increases closely to the center of the pipe.[8] The impact of inertial particles on the turbulent kinetic energy and turbulent kinetic energy dissipation in particle-laden flows were quantified.[9] By use of the PIV instrument, the presence of particles noticeably alters the carrier phase turbulence properties through an effective increase in the wall friction velocity of approximately 7% and an increase in normal and shear Reynolds stress by approximately 8−10% in the outer flow.[10] Particle inertia are of great importance for gas turbulence modification, even if the lower mass loading ratio of 5×10^{-4}. It was attenuated with increasing particle size and mass loadings.[11] Swirling two-phase hydrodynamics using PDPA were also performed.[12,13] In recent years, the direct numerical simulation (DNS),[18−23] the large eddy simulation (LES), and[24−30] the Reynolds averaged Navier−Stokes simulation (RANS)[31−40] have been rapidly applied to model and simulate the hydrodynamics of two-phase flows based on the computational fluid dynamics (CFD) technique. The definition of gas turbulence modulation in particle-laden flows can be expressed by the effects of the relevant particle size, density, and volume fraction on flow information as well as the

Received: January 6, 2021
Accepted: March 24, 2021
Published: April 5, 2021

https://doi.org/10.1021/acsomega.1c00085
ACS Omega 2021, 6, 10106−10118

Table 1. Mathematical Model of the Gas−Particle Swirling Flow in the Chamber

A: conservation equations

(a) continuity equations

gas phase

$$\frac{\partial}{\partial t}(\alpha_g\rho_g) + \frac{\partial}{\partial x_j}(\alpha_g\rho_g\overline{u_{gi}}) = 0 \quad \text{(T1)}$$

particle phase

$$\frac{\partial}{\partial t}(\alpha_s\rho_s) + \frac{\partial}{\partial x_j}(\alpha_s\rho_s\overline{u_{si}}) = 0 \quad \text{(T2)}$$

(b) momentum equations

gas phase

$$\frac{\partial(\alpha_g\rho_g\overline{u_{gi}})}{\partial t} + \frac{\partial(\alpha_g\rho_g\overline{u_{gk}u_{gi}})}{\partial x_k} = \alpha_g\rho_g g - \alpha_g\frac{\partial\overline{p}}{\partial x_i} + \frac{\partial}{\partial x_k}(\tau_{gik} - \alpha_g\rho_g\overline{u'_{gi}u'_{gk}}) + \beta_{gs}(\overline{u_{si}} - \overline{u_{gi}}) \quad \text{(T3)}$$

particle phase

$$\frac{\partial(\alpha_s\rho_s\overline{u_{si}})}{\partial t} + \frac{\partial(\alpha_s\rho_s\overline{u_{sk}u_{si}})}{\partial x_k} = \alpha_s\rho_s g - \alpha_s\frac{\partial\overline{p_g}}{\partial x_i} - \frac{\partial\overline{p}}{\partial x_i} - \frac{\partial}{\partial x_k}(\tau_{sij} - \alpha_s\rho_s\overline{u'_{sk}u'_{si}}) + \beta_{sg}(\overline{u_{si}} - \overline{u_{gi}}) \quad \text{(T4)}$$

(c) equation of particle fluctuating energy

$$\frac{3}{2}\left[\frac{\partial(\alpha_s\rho_s\theta)}{\partial t} + \frac{\partial(\alpha_s\rho_s\overline{u_{sk}}\theta)}{\partial x_k}\right] = \frac{\partial}{\partial x_k}\left(C_s\alpha_s\rho_s\frac{\kappa_s^2}{\varepsilon_s}\right) + \frac{\partial}{\partial x_k}\left(\kappa_s\frac{\partial\theta}{\partial x_k}\right) + \mu_s\left(\frac{\partial\overline{u_{sk}}}{\partial x_i} + \frac{\partial\overline{u_{si}}}{\partial x_k}\right)\frac{\partial\overline{u_{si}}}{\partial x_k} + \mu_s\varepsilon_s - \overline{p}_s\frac{\partial\overline{u_{sl}}}{\partial x_l} + \left(\xi_s - \frac{2}{3}\mu_s\right)\left(\frac{\partial\overline{u_{sl}}}{\partial x_l}\right)^2 - \gamma_s \quad \text{(T5)}$$

B: constitutive equations

(a) Reynolds stress equation of gas phase

$$\frac{\partial(\alpha_g\rho_g\overline{u'_{gi}u'_{gj}})}{\partial t} + \frac{\partial(\alpha_g\rho_g\overline{u_{gk}}\cdot\overline{u'_{gi}u'_{gj}})}{\partial x_k} = D_{g,ij} + P_{g,ij} + \Pi_{g,ij} - \varepsilon_{g,ij} + \sum_{s=1}^{M} G_{g,gs,ij} \quad \text{(T6)}$$

(b) Reynolds stress equation of particle phase

$$\frac{\partial(\alpha_s\rho_s\overline{u'_{si}u'_{sj}})}{\partial t} + \frac{\partial(\alpha_s\rho_s\overline{u_{sk}}\cdot\overline{u'_{si}u'_{sj}})}{\partial x_k} = D_{s,ij} + P_{s,ij} + \Pi_{s,ij} - \varepsilon_{s,ij} + \sum_{s=1}^{M} G_{s,gs,ij} \quad \text{(T7)}$$

(c)turbophoresis force

$$D_{s,ij} = \frac{\partial}{\partial x_k}\left(C_p\alpha_s\rho_s\frac{k_s}{\varepsilon_s}\overline{u'_{sk}u'_{sl}}\frac{\partial\overline{u'_{si}u'_{sj}}}{\partial x_l}\right) \quad \text{(T8)}$$

(d) particle shear production

$$P_{s,ij} = -\alpha_s\rho_s\left(\overline{u'_{sk}u'_{sj}}\frac{\partial\overline{u_{si}}}{\partial x_k} + \overline{u'_{sk}u'_{si}}\frac{\partial\overline{u_{sj}}}{\partial x_k}\right) \quad \text{(T9)}$$

(e) particle pressure−strain

$$\prod_{s,ij} = \prod_{s,ij,1} + \prod_{s,ij,2} = -C_{p1}\frac{\varepsilon_s}{k_s}\alpha_s\rho_s\left(\overline{u'_{si}u'_{sj}} - \frac{2}{3}k_s\delta_{ij}\right) - C_{p2}\left(P_{s,ij} - \frac{2}{3}P_s\delta_{ij}\right) \quad \text{(T10)}$$

(f) particle dissipation

$$\varepsilon_{s,ij} = \frac{2}{3}\delta_{ij}\alpha_s\rho_s\alpha_s \quad \text{(T11)}$$

(g) two-phase interaction

$$\sum_{s=1}^{M} G_{s,gs,ij} = \frac{\alpha_s\rho_s}{\tau_{rs}}(\overline{u'_{si}u'_{gj}} + \overline{u'_{gj}u'_{si}} - 2\overline{u'_{si}u'_{sj}}) \quad \text{(T12)}$$

(h) equation of gas−particle interphase Reynolds stress

$$\frac{\partial\overline{u'_{si}u'_{gj}}}{\partial t} + (\overline{u_{gk}} + \overline{u_{sk}})\frac{\partial\overline{u'_{si}u'_{gj}}}{\partial x_k} = D_{gs,ij} + P_{gs,ij} + \Pi_{gs,ij} - \varepsilon_{gs,ij} + T_{gs,ij} \quad \text{(T13)}$$

(i) interphase diffusion

$$D_{gs,ij} = \frac{\partial}{\partial x_k}\left(C_{gs3}\left(\frac{k_s}{\varepsilon_s}\overline{u'_{pk}u'_{pl}} + \frac{k_g}{\varepsilon_g}\overline{u'_{gk}u'_{gl}}\right)\frac{\partial\overline{u'_{gi}u'_{sj}}}{\partial x_l}\right) \quad \text{(T14)}$$

(j) interphase shear production

$$P_{gs,ij} = -\overline{u'_{si}u'_{gk}}\frac{\partial\overline{u_{gj}}}{\partial x_k} - \overline{u'_{sk}u'_{gj}}\frac{\partial\overline{u_{si}}}{\partial x_k} \quad \text{(T15)}$$

(k) interphase pressure−strain

$$\prod_{gs,ij} = \prod_{gs,ij,1} + \prod_{gs,ij,2} = -\frac{C_{gs,1}}{\tau_{rs}}\left(\overline{u'_{si}u'_{gj}} - \frac{2}{3}k_{gs}\delta_{ij}\right) - C_{gs,2}\left(P_{gs,ij} - \frac{2}{3}P_{gs}\delta_{ij}\right) \quad \text{(T16)}$$

(l) interphase dissipation

$$\varepsilon_{gs,ij} = \frac{\overline{u'_{si}u'_{gj}}}{\min(\tau_{rs}, k_s/\varepsilon_s)} \quad \text{(T17)}$$

(m) interphase interaction

$$T_{gs,ij} = \frac{\beta}{\alpha_g\rho_g\alpha_s\rho_s}(\alpha_s\rho_s\overline{u'_{si}u'_{sj}} + \alpha_g\rho_g\overline{u'_{gi}u'_{gj}} - (\alpha_g\rho_g + \alpha_s\rho_s)\overline{u'_{gj}u'_{si}}) \quad \text{(T18)}$$

https://doi.org/10.1021/acsomega.1c00085
ACS Omega 2021, 6, 10106−10118

Table 1. continued

B: constitutive equations

(n) conductivity coefficient of granular temperature

$$\kappa_s = \frac{150}{384(1+e)g_0}\rho_s d_s\sqrt{\pi\theta}\left[1+\frac{6}{5}(1+e)g_0\alpha_s\right]^2 + 2\alpha_s^2\rho_s d_s g_0(1+e)\sqrt{\frac{\theta}{\pi}} \quad \text{(T19)}$$

(o) translational fluctuation energy dissipation rate

$$\gamma_s = 3(1-e^2)\alpha_s^2\rho_s g_0\theta\left[\frac{4}{d_p}\sqrt{\frac{\theta}{\pi}} - \frac{\partial u_{k,s}}{\partial x_k}\right] \quad \text{(T20)}$$

(p) bulk particle viscosity

$$\xi_s = \frac{4}{3}\alpha_s^2\rho_s d_s g_0(1+e)\sqrt{\frac{\theta}{\pi}} \quad \text{(T21)}$$

(q) Radial distribution function

$$g_0 = \left[1-\left(\frac{\alpha_s}{\alpha_{s,max}}\right)^{1/3}\right]^{-1} \quad \text{(T22)}$$

(r) particle relax time

$$\tau_{rs} = d_s^2\rho_s\left(1+\frac{Re_s^{2/3}}{6}\right)^{-1}/18\mu_g \quad \text{(T23)}$$

(s) particle viscosity

$$\mu_s = \frac{10\rho_s d_s\sqrt{\pi\theta}}{96\alpha_s(1+e)g_0}\left[1+\frac{4}{5}(1+e)g_0\alpha_s\right]^2 + \frac{4}{5}\alpha_s^2\rho_s d_s g_0(1+e)\sqrt{\frac{\theta}{\pi}} + \mu_s^f \quad \text{(T24)}$$

frictional stress

$$\mu_s^f = \frac{p_s^f \sin\varphi_f}{2\sqrt{I_{2D}}} \quad \text{(T25)}$$

$$I_{2D} = -\frac{1}{2}\left[\frac{1}{2}(\nabla u_s + \nabla u_s^T) - \frac{1}{3}(\nabla\cdot u_s)I\right]:\left[\frac{1}{2}(\nabla u_s + \nabla u_s^T) - \frac{1}{3}(\nabla\cdot u_s)I\right] \quad \text{(T26)}$$

$$p_s^f = \begin{cases} 0.05\dfrac{(\alpha_s-\alpha_{s,min})^2}{(\alpha_{s,max}-\alpha_s)^5} & \alpha_s > \alpha_{s,min} \\ 0 & \alpha_s \le \alpha_{s,min} \end{cases} \quad \text{(T27)}$$

(t) interphase momentum exchange coefficient

Ergun model

$$\beta_{Ergun} = 150\frac{\alpha_s(1-\alpha_g)\mu_g}{\alpha_g(\varphi d_s)^2} + 1.75\frac{\alpha_s\rho_g|\overline{u_g}-\overline{u_s}|}{\varphi d_s} \quad \text{(T28)}$$

Wen-Yu model

$$\beta_{Wen,Yu} = \frac{3}{4}C_D\frac{\alpha_s\alpha_g\rho_g|\overline{u_g}-\overline{u_s}|}{d_s}\alpha_g^{-2.65} \quad \text{(T29)}$$

Huilin-Gidaspow model

$$\beta_{sg} = (1-\phi)\beta_{Ergun} + \phi\beta_{Wen\text{-}Yu} \quad \text{(T30)}$$

$$\phi = \frac{\arctan[150\times 1.75(0.2-\alpha_s)]}{\pi} + 0.5 \quad \text{(T31)}$$

$$C_D = \frac{24}{Re_s}(1+0.15Re_s^{0.687}) \qquad Re_s \le 1000 \quad \text{(T32)}$$

$$C_D = 0.44 \qquad Re_s > 1000 \quad \text{(T33)}$$

particle Reynolds number

$$Re_s = \frac{\alpha_g\rho_g d_s|\overline{u_g}-\overline{u_s}|}{\mu_g} \quad \text{(T34)}$$

particle Stokes number even if it has been not well understood so far. Turbulence modification was characterized into augmentation and attenuation categories using a developed intuitive parameter, which is the ratio of the particle diameter to a characteristic size of large eddies.[41] The threshold of particle volume fraction (α) to characterize effects of particle on gas turbulence was firstly proposed, that is the one-way coupling ($\alpha < 10^{-6}$), the two-way coupling ($10^{-6} < \alpha < 10^{-3}$), and the four-way coupling ($\alpha > 10^{-3}$).[42] By using the DNS algorithm, gas turbulence was attenuated by fine particles in developing the boundary layer and fully developed channel flows when mass loading ratios are greater than 10%.[18] Turbulence modulation is more highly sensitive to the effect of mass loading rather than the particle response.[19] Also, it is determined by a group of parameters rather than a sole factor, that is, combination of swirling number, mass loading, particle size and density, and so forth, in which mass loading was considered as the leader order. Moreover, turbulent kinetic energy depends on the intermediate and the small-scale vortices are smaller than those of in single swirling jet.[20,21] Low-inertia particles trigger the laminar-to-turbulent instability, whereas high-inertia particles tend to stabilize turbulence due to the extra dissipation induced by particle−fluid coupling.[22] Regarding the LES application, turbulence modulations have strongly anisotropic characteristics and been closely determined by the flow structure in the backward facing step two-phase flows, especially smaller size and lower density particle enhanced the turbulence modulation.[23] For the first time, the swirling particle-laden follows in a coaxial-jet combustor were numerically simulated.[24,25] The two-phase hydrodynamics, that is, particle dispersion characteristics, particle residence time of different particle sizes, evolution coherent structures, and particle−diameter correlation were obtained. However, the trend gas turbulence modulations by

https://doi.org/10.1021/acsomega.1c00085
ACS Omega 2021, 6, 10106−10118

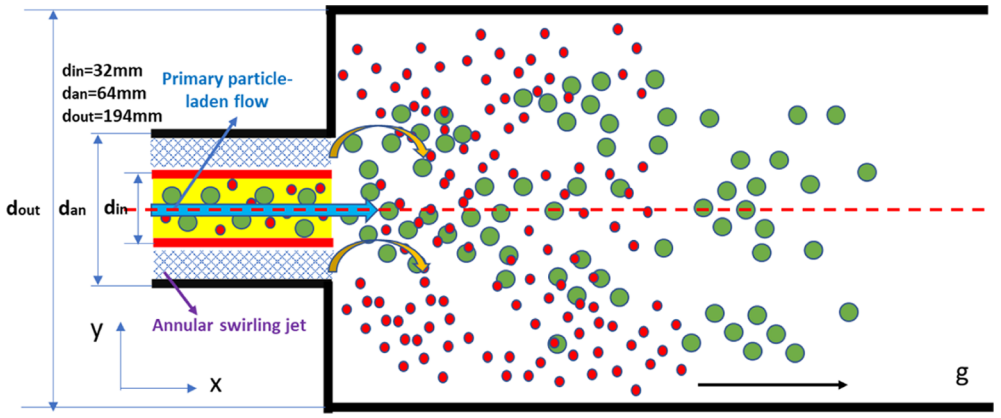

Figure 1. Schematic diagram of a coaxial swirling chamber.

the particle have not been provided completely. Experimental data to validate the DNS results are virtually nonexistent due to the complexity of gas−particle two-phase turbulent flows and the current measurement approaches.[30] In regard to the LES algorithm, the most challenge is that how to establish the accurate subgrid scale (SGS) models and carry out the priori verifications. Compared to DNS and LES, RANS is the compromised way due to economic computation, robust turbulent model, and practically empirical coefficient, even if it failed to disclose the instantaneous flow behavior and coherent turbulent structure. A standard $k-\varepsilon$ two-equation turbulence was used to model the effects of particle size, mass loading, and swirling number on gas turbulence modulation at the internal recirculation region.[31] The gas phase solved by a standard $k-\varepsilon$ turbulence mode and discrete particle models for tracking the particle trajectory in swirling two-phase turbulence flow was also studied.[32] A developed $k-\varepsilon$ particle collision model for dilute gas−particle vertical flows containing high-inertia particles was carried out, indicating that the interparticle length scale has a significant effect on gas turbulence.[33] A new dimensionless particle moment number of particle-laden Navier−Stokes equations was established to identify turbulence attenuation between the augmentation regions with two critical particle momentum numbers according to the mapped of Re−Pa numbers.[34] A probability density function to describe the cylindrical particle orientation was developed. Turbulence intensity enhancement caused by cylindrical particles in the streamwise is smaller than that of near the nozzle exit, as well as directly proportional to particle concentration, Reynolds number, and particle aspect ratio.[35] A two-phase turbulent Reynolds stress model to predict the swirling particle dispersions in behind a sudden tube expansion was improved for simulation; results show that the fine particle attenuates the gas turbulence of up 25%.[36] A series of the second-order moment gas−particle and gas−liquid turbulent models to simulate the anisotropic dispersions of particle and bubble, and hydrodynamics of gas−particle, and bubble-particle two-phase flows were developed to successfully reveal the anisotropic characteristics, the redistributions of Reynolds stresses of two phases, and the mixing and separation behaviors.[37−43]

Until now, the mechanism of turbulence modulation by particles in swirling gas−particle flows has not been clarified clearly. The aim of the present study is to explore the turbulence modulations by the effects of particle density and size, the Stokes number using ultralight expanded graphite (EG), and heavy copper particles. A second-order moment gas−particle turbulence model was developed, which the Reynolds stress transport equation and the particle temperature equation based on the kinetic theory of granular flow are used to describe the anisotropic characteristics and particle−particle collisions. The measurement data of glass bead in experiments were used to validate the proposed mathematical model, algorithm, and in-house code.[13] Effects of particles on gas turbulence modulations are analyzed in detail.

COMPUTATIONAL METHODS

The gas and the dispersed particle phases are modeled by the Eulerian−Eulerian two-fluid approach, which treats both the gas and particulate phase as each continuous medium. It involves the solution of a two-phase set of Navier−Stokes equations using the four-way coupling correlation, indicating the interactions of gas−particle and particle−gas. Particle−particle collisions are completely considered. Particularly, the anisotropic characteristics of particle dispersions were modeled by an improved the two-phase Reynolds stress transport equations and particle temperature equation. Conservation laws of mass and momentum are satisfied for each phase; no mass and heat transfer occurred between gas and particle phases. The governing equations are summarized as in Table 1.

Experimental Setting. The coaxial cylindrical chamber in an experiment consists of the primary core zone and the secondary annual jet zone. Diameters of the primary inject, annulus jet, and main outer chamber are 32.0, 64.0, and 194.0 mm, respectively. The total length test section that is oriented vertically with the gravity acting in the direction of the flow is 960.0 mm. Predictions are laden with the ultralight expanded graphite (EP) and the copper beads with a density of 21.9 and 8900.0 kg/m^3 with each diameter of 45.0 and 1000.0 μm, respectively. Glass beads are used to verify the simulation result, which have 2500.0 kg/m^3 density and are 45 μm in diameter with Stokes number St = 0.025. As for the gas phase, the initial primary central flow rate is 9.9 g/s, the initial annular flow rate is 38.3 g/s, and the inlet Reynolds number is 52,400. The particle mass flow rate is 0.34 g/s and the particle loading in the primary flow η is 0.034, which is defined as the ratio of the particle to gas phase mass flow rates in eq 1. The mass flow rates correspond to the particle inertia leading to the different effects on inlet flow structures. Larger inertia particles are easier to be entrained to the primary central regions instead of secondary flow regions.

https://doi.org/10.1021/acsomega.1c00085
ACS Omega 2021, 6, 10106−10118

$$\eta = \frac{\dot{m}_s}{\dot{m}_g} = \frac{\rho_s u_s}{\rho_g u_g} \quad (1)$$

The swirling number is set to 0.47 in this simulation (see eq 2). The date output positions are obtained at the length of 3.0, 52.0, 155.0, 195.0, and 315.0 mm along the streamwise directions. Detailed schematic diagrams are shown in Figure 1.

$$s = \frac{2\int_0^{d_a} \rho_g w_g u_g r^2 dr}{d_a \int_0^{d_a} \rho_g u_g^2 dr} \quad (2)$$

where s is the abbreviation of swirling number, a is the annular jet, r is the radius, d_a is the diameter of the annular jet, u_g and w_g are the axial and tangential gas velocity, respectively, and ρ_g is the density of gas phase. A dimensionless parameter, Stokes number St, is defined by $St = \tau_s/\tau_f$ as eqs 3 and 4, which is used to classify the degree of the particle entrainment into the gas flow. τ_s is the particle relaxation time and τ_f is the fluid time scale, respectively.

$$\tau_s = \frac{1}{18}\frac{\rho_s d_s^2}{\mu_g} \quad (3)$$

$$\tau_f = \frac{d_{in}}{u_{jet}} \quad (4)$$

$$St = \frac{\tau_s}{\tau_f} = \frac{1}{18}\frac{\rho_s d_s^2 d_{in} u_{jet}}{\mu_g} \quad (5)$$

The experimental parameters and simulation settings are given as Table 2. Moreover, the interim value of St = 1.11 in between 43.6 and 0.002 using copper particles with diameter of 160.0 μm is also simulated to investigate the trend of the effect of Stokes number in-between on turbulence modulations.

Numerical Algorithm. The finite volume method and the staggered grid technique are utilized to solve transport equations and Reynolds stress models in a generalized coordinate space. The quadratic upstream interpolation for convective kinematics procedure and the central difference scheme (CDS) for the diffusion terms are employed as well. The computational domain is first divided into a finite number of control volumes and then was integrated over this certain control volume. The semi-implicit for pressure linked equation correction, the tri-diagonal marching algorithm, the line-by-line iteration, and the under-relaxation are served for the velocity corrections to meet the requirements of continuity criteria, which are set to the of 1.0×10^{-4} for residual mass sources. The uniform and parabolic distributions for gas and particle inlet velocity, the isotropic profiles for normal components of Reynolds stresses, and the eddy viscosity hypothesis for shear stress are set up. Values of initial values of the particle temperature are defined by $\theta = 0.005u^2_{p,in}$, and inlet dissipation is $\varepsilon_{in} = c_\mu^{0.75} k_{in}^{1.5}/\lambda L$. Nonslip wall conditions are set for gas velocity and the gas Reynolds stresses were determined by the production terms. The tangential particle velocity and granular temperature at the wall are calculated.[44] In-house computational codes are compiled by the Fortran 77 consisting of approximately 22,000 statements.

$$u_{s,wall} = -\frac{6\mu_s \alpha_{s,max}}{\pi \rho_s \alpha_s g_0 \sqrt{3\theta}} \frac{\partial u_{s,wall}}{\partial n} \oplus \quad (6)$$

Table 2. Parameters of the Experiment and Numerical Simulation

parameters	Unit	value
diameter of expanded graphite and copper particles, d_s	mm	45/1000
45, 160/1000		
density of expanded graphite and copper particles, ρ_s	kg/m^3	21.9, 8900
diameter of the glass bead for CFD validation, d_{sb}	mm	45
density of the glass bead for CFD validation, ρ_{sb}	kg/m^3	2500
density of gas, ρ_g	kg/m^3	1.225
viscosity of gas, μ_g	Pa.s	1.8×10^5
restitution coefficient of particle−wall, e_w		0.96
restitution coefficient of particle−particle, e		0.95
particle sphericity, φ		0.96
diameter of the primary inject, d_{jn}	mm	32
diameter of the annular jet, d_{an}	mm	64
diameter of the chamber, d_o	mm	194
total length, L	mm	960
particle loading, η		0.034
swirling number, s		0.47
flow rate in the primary jet, $\dot{m}_s$	g/s	9.9
flow rate in the annular jet, $\dot{m}_{an}$	g/s	38.3
inlet Reynolds number, Re_{in}		52,400
Stokes numbers of copper St, d_s = 45,160,1000 μm		0.087, 1.11, 43.6
Stokes numbers of expanded graphite St, d_s = 45,1000 μm		0.0002, 0.11
Stokes number of the glass bead for CFD validation St, d_s = 45 μm		0.025

$$\theta_{wall} = -\frac{k_s \theta}{e_w}\frac{\partial \theta_{wall}}{\partial n} + \frac{\sqrt{3}\pi \rho_s \alpha_g u_s g_0 \theta^{3/2}}{6\alpha_{s,max} e_{wall}} \quad (7)$$

RESULTS AND DISCUSSION

Experimental Validations. The mathematical model, numerical algorithm, and in-house code were validated by experimental measurements using glass beads with a density of 2500.0 kg/m^3 and diameter of 45.0 μm.[13] The grid independence for the axial particle velocity by means of coarse (6.0 × 1.9 mm), medium (2.0 × 0.48 mm), and fine (1.3 × 0.33 mm) grid sizes was tested (see Figure S1). A medium grid size is acceptable due to the economic CPU time and satisfied results that adopted for the grid scheme. The swirling flow exhibits considerable anisotropy, especially in the shear layer and flow core regions. Concerning the key flow features including the primary corner and secondary recirculation zones with cores that centered at the (x,r) coordination of (117.4,

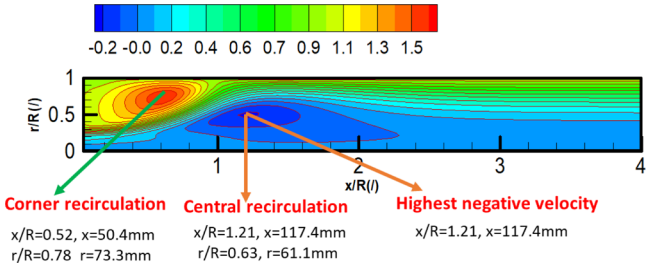

Figure 2. Predictions of gas−particle flow characteristics using the glass bead experiment.

https://doi.org/10.1021/acsomega.1c00085
ACS Omega 2021, 6, 10106−10118

Table 3. Comparison with LES and Experimental Data

	in this simulation	LES	experiment data
primary circulation zone, (x, r)	(50.4, 73.3 mm)	(49.8, 76.8 mm)	(52.0 mm,/)
secondary circulation zone, (x, r)	(117.4, 61.1 mm)	(115.4, 64.0 mm)	(112.0 mm,/)_
reattachment point, (x, r)	(53.8, 93.0 mm)	(52.2, 94.7 mm)	(52.0 mm,/)
maximum relative error with experiments, %	4.8	3.1	

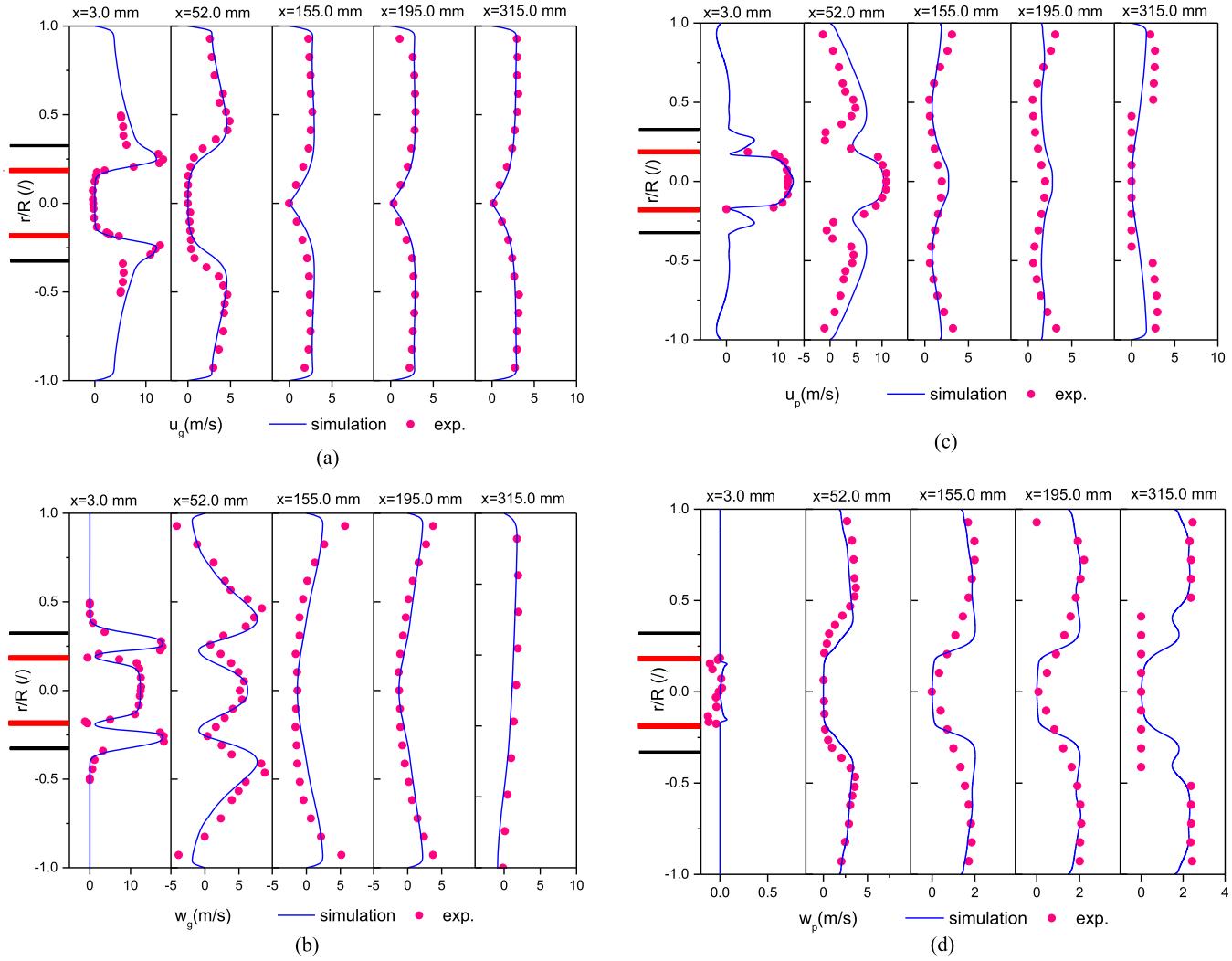

Figure 3. Validation of the time-averaged axial and tangential velocities of gas and particles using the glass bead experiment, St = 0.025:[13] (a) axial direction, gas; (b) tangential direction, gas; (c) axial direction, particle; and (d) tangential direction, particle.

61.1 mm) and (50.4, 73.3 mm), the reattachment point centered at approximately (53.8, 93.0 mm), and the highest negative velocities within the primary recirculation region is found at the coordinates of x = 117.4 mm, respectively (see Figure 2 and Table 3).These values complied with the measured results by ref 13 within 5% errors as well as the LES simulations by refs 24, 25. Predictions of axial and tangential two-phase velocities at the streamwise sections in comparison with the PDPA data are shown in Figure 3. The W-shaped profiles at annular flow regions and the typical Rankine vortex structure along the axial tangential direction are captured in the shear layers, respectively. These findings correlate well with the experimental results even if they have slightly overestimated at the near wall zone at x = 155.0 mm. The errors mainly are caused by the time-averaged method in this research because it fails to capture the instantaneous flow information, coherent structure of turbulent flow, especially for the evolution of vortex stretch, as shown in distinct vortex regions in Figure 3. Although LES and DNS algorithms may overcome these drawbacks to some degree, it was confined strictly by the accurate SGS models, wall boundaries, and unaffordable CPU time.[24−26,30,31,37]

Turbulent Modulations by Particles. Figures 4 and 5 demonstrate the distributions of gas streamlines and vorticities with a large span of Stokes number values ranging from St = 0.0002 to St = 43.6. As we can see streamlines have significantly been changed because of the effect of the sudden expansion of the geometry section. Two typical recirculating regions were observed, that is, a central primary jet region at the near-axial region as a result of the appearance of return flow with a negative velocity and a corner recirculating region at the wall-bound region as a result of the two-phase flow

https://doi.org/10.1021/acsomega.1c00085
ACS Omega 2021, 6, 10106−10118

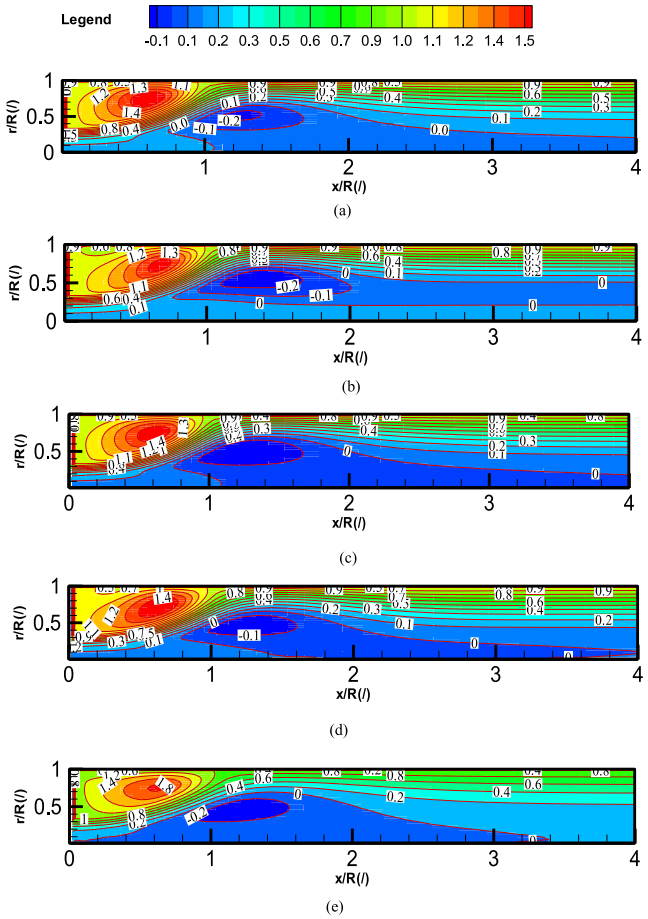

Figure 4. Modulations of the gas streamline by particles: (a) unladen particle, St = 0.025; (b) ultralight particle, d = 45.0 μm, St = 0.0002; (c) ultralight particle, d = 1000.0 μm, St = 0.11; (d) heavy particle, d = 45.0 μm, St = 0.087; and (e) heavy particle, d = 1000.0 μm, St = 43.6.

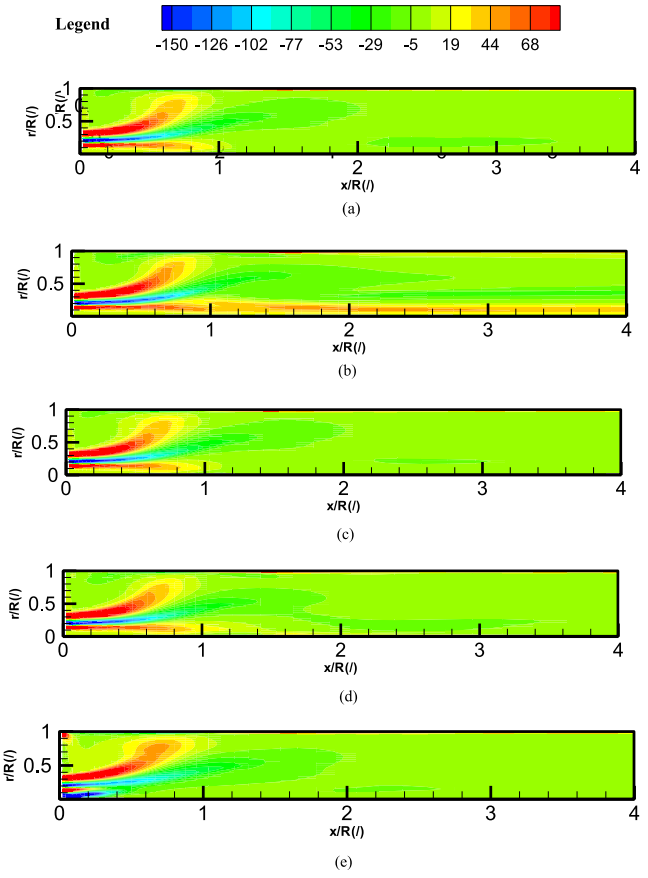

Figure 5. Modulations of gas vorticities by particles (1/s, $r-w$ plane): (a) unladen particle; (b) ultralight particle, d = 45.0 μm, St = 0.0002; (c) ultralight particle, d = 1000.0 μm, St = 0.11; (d) heavy particle, d = 45.0 μm, St = 0.087; and (e) heavy particle, d = 1000.0 μm, St = 43.6.

reattachment production under the combination effects of sudden expansion, turbophoresis force, and particle inertia. The density and the diameter of particles are given as a function of Stokes number, and they greatly impacted on the evolution processes of flow and vortex structures. When the Stokes number is far less than unity, it means that the particles are well entrained into the gas turbulence. These have excellent followability in the carrier gas, and the two-phase flow could be treated as a homogeneous phase. Especially, particles are significantly responsive to gas fluctuations. When the Stokes number is greater than unity, particles are unresponsive to gas−phase fluctuations and move unaffected through the gas eddies due to large inertia of the particle. Table 4 indicates the effects of particles on flow characteristics under different Stokes number values. Ultralight particles quickly respond to gas flow in recirculation leading to more entrainment in the secondary recirculation zone due to strong followability.

As shown in Figure 5, shedding vortices from the inlet region that rolled up by the boundary layer with vortices from the shear layer underwent a process of pairing, merging, and breakup. Large-heavy particles are easier to penetrate the central reversed flow regions instead of undergoing toward the wall-normal region due to the large inertia and lagging velocity with gas inlet velocity. Therefore, distinctly vortex structures were not generated because of the perturbance of inertia particles. In order to consider the effects of in-between or interim Stokes number values, St = 1.11 using heavy particles with a diameter of d_s = 160.0 μm was introduced (see Figure S2). The flow status shows the apparently transition characteristics in terms of primary and secondary circulation, vortex evolution, and so forth.

Modulations of Mean Velocities by Particles. Figure 6 shows the axial, radical, and tangential gas mean velocity modulations by particles. Negative velocities can be observed at the near centerline and wall recirculation regions except for the tangential swirling velocity. The decay of axial velocities occurs along the streamwise centerline and the trend to shift toward the wall region reaching up to a maximum are disclosed. Radial velocities at a central flow have the maximum values, and they decrease in the boundary of the primary jet. Meanwhile, significantly decreasing peaks along the streamwise direction and flattened profiles over the cross sections are presented with a similar trend of tangential velocities. With the disappearance of the inlet effect, velocities have seriously changed after the streamwise section of x = 155.0 mm, and effects of smaller Stokes number on axial and tangential velocities can be negligible even at the near inlet region. As a matter of the fact, the attenuation of gas turbulence by heavy-large particles is remarkable. At the near inlet region, light-small particles were subjected to be thrown out from the central reversed flow zone, which then moved toward the outer region by the centrifugal force. In sharp contrast, intensified

https://doi.org/10.1021/acsomega.1c00085
ACS Omega 2021, 6, 10106−10118

Table 4. Comparison of Hydrodynamic Characteristics of Particles

	ultralight particle		heavy particle	
	d_s = 45.0 μm	d_s = 1000.0 μm	d_s = 45.0 μm	d_s = 1000.0 μm
Stokes number	0.0002	0.11	0.087	43.6
followability	excellent	good	excellent	worse
second recirculation	entrainment	entrainment	entrainment	penetration
length of the primary and secondary circulation	enlarge	enlarge	enlarge	weak
preferential accumulation	increase	increase	increase	decrease
vortex formation	helpful	helpful	unhelpful	destructive

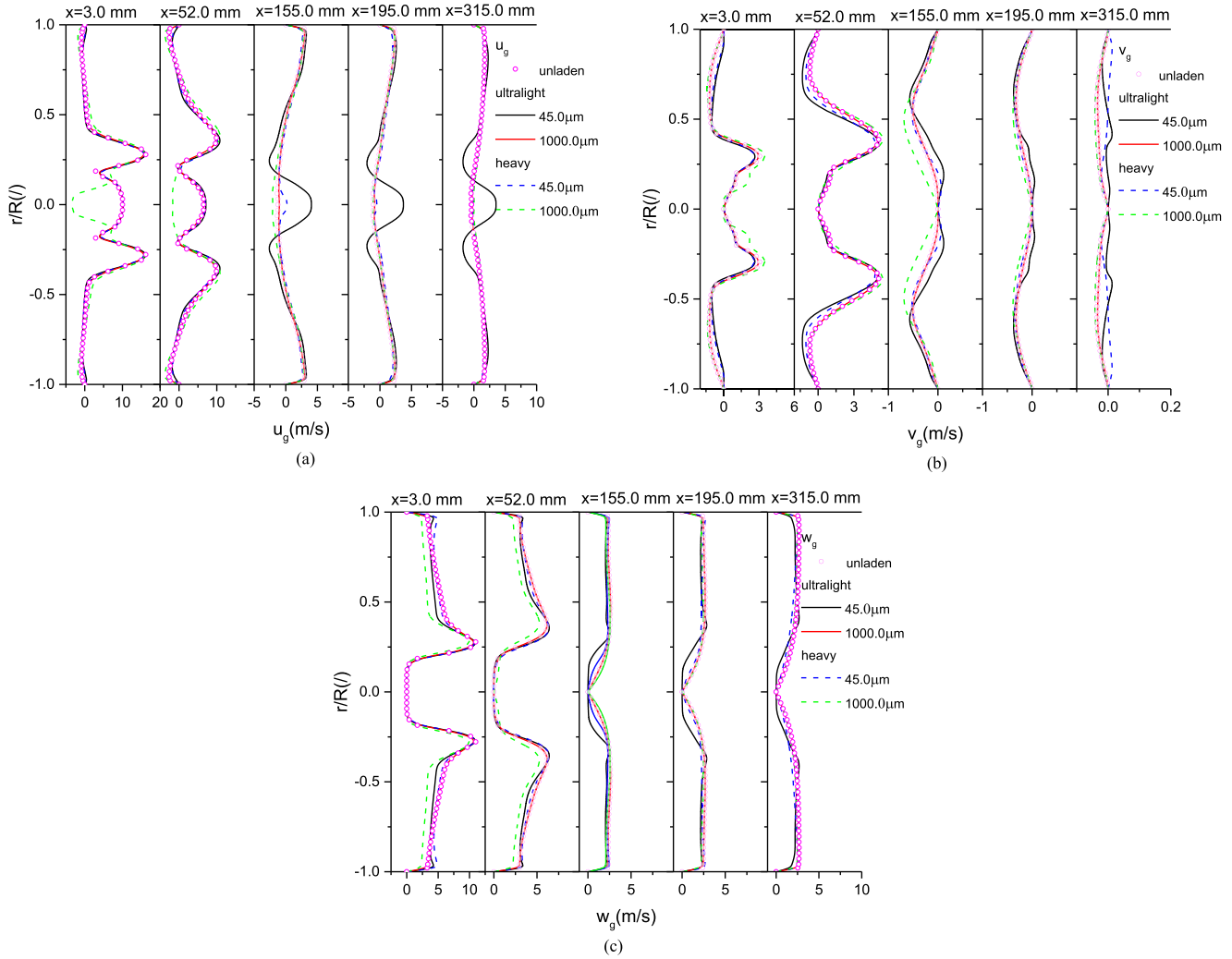

Figure 6. Modulations of gas mean velocities by particles: (a) axial direction; (b) radial direction; and (c) tangential direction.

modulations by heavy-large particles with a high Stokes number exert great effects on gas turbulence modulation due to higher lagging velocity and inertia. At the far downstream locations, axial velocities are significantly enhanced; however, radial and tangential velocities are weakened even with a small Stokes number. Moreover, preferential accumulations of light particles are weaker than those of heavy particles at the section of x > 155.0 mm because of the anisotropic dispersions and excellent followability. The behaviors of the transition particle with St = 1.11 are close to those of the heavy-large particle which is adjacent to the threshold of St = 1.0 (see Figure S3).

Modulations of Root-Mean-Square Fluctuation Velocities by Particles. Figure 7 shows the modulation of the root-mean-square (rms) fluctuation velocities of gas turbulence by laden particles, which is defined by $\overline{u_g'} = \sqrt{(u_g')^2}$. Significant anisotropic characteristics of gas fluctuations are observed in the shear regions, in which the corresponding highest velocity gradient decreases toward the centerline and the jet boundary. With the development of flow, modulations by particles seems to weaken than those of near inlet regions due to lower local particle mass flux. Larger Stokes numbers always strengthen the modulations in contrast to the smaller Stokes number of light-small particles because of the different history experiences. Considering the effect of initial inertia, particles first are entrained into the central recirculating zone than being gradually decelerated, stopped, and turned backward flow. Radial and tangential velocities became more dominantly, and

https://doi.org/10.1021/acsomega.1c00085
ACS Omega 2021, 6, 10106−10118

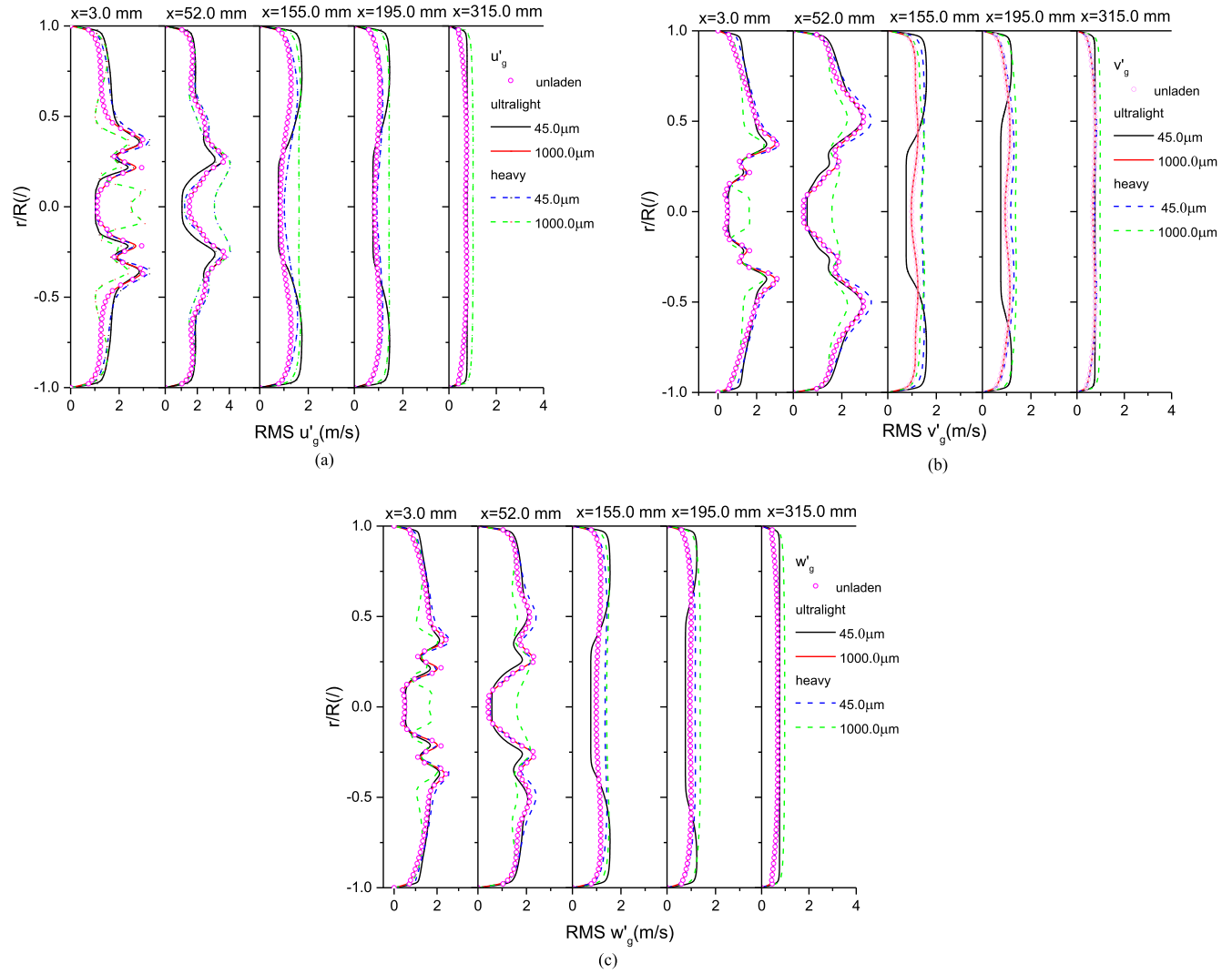

Figure 7. Modulations of gas rms fluctuation velocities by particles: (a) axial direction; (b) radial direction; and (c) tangential direction.

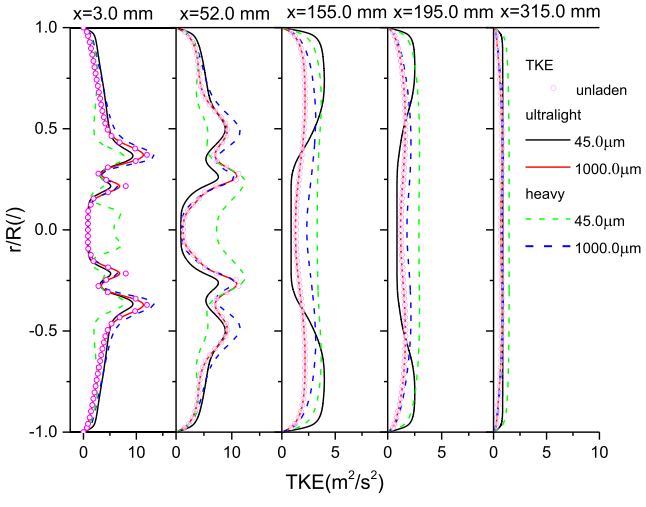

Figure 8. Modulation of gas TKE by particles.

particles gradually move toward the wall driven by centrifugal force. Light-small particles with small Stokes number are strongly controlled and decelerated by reversal flow in the primary recirculating jet as a result of a decrease in central fluctuations. Heavy-large particles with high Stokes number reinforce the turbulence fluctuations at every direction. The compromise characteristics of modulations for St = 1.11 are provided in Figure S4.

Modulations of Turbulence Kinetic Energy by Particles. Modulation of turbulence kinetic energy (TKE) by particles is given in Figure 8, which is defined as $\mathrm{TKE} = \frac{1}{2}(\overline{u_g'^2} + \overline{v_g'^2} + \overline{w_g'^2})$. The enhancement at centerline regions by heavy particles and those at near-wall regions by light particles after the section of $x > 155.0$ mm is obtained. Noticeably, the degree of modulation of light particles is larger than that of heavy particles due to quick absorption of the kinetic energy from different flow processes. The particle trajectory, slip velocity, and drag force transferred to the gas phase are all uniquely determined by the particle time constant or Stokes number at a large ratio of particle to fluid material density when particle diameters are approximately smaller than the Kolmogorov scale. When the diameter of particle is smaller than the Kolmogorov scale, it has a small distortion to moderate scale turbulent eddies.[45,46] Thus, particles with the same Stokes number including different diameters and densities to modulate gas turbulence may conduct the different

https://doi.org/10.1021/acsomega.1c00085
ACS Omega 2021, 6, 10106−10118

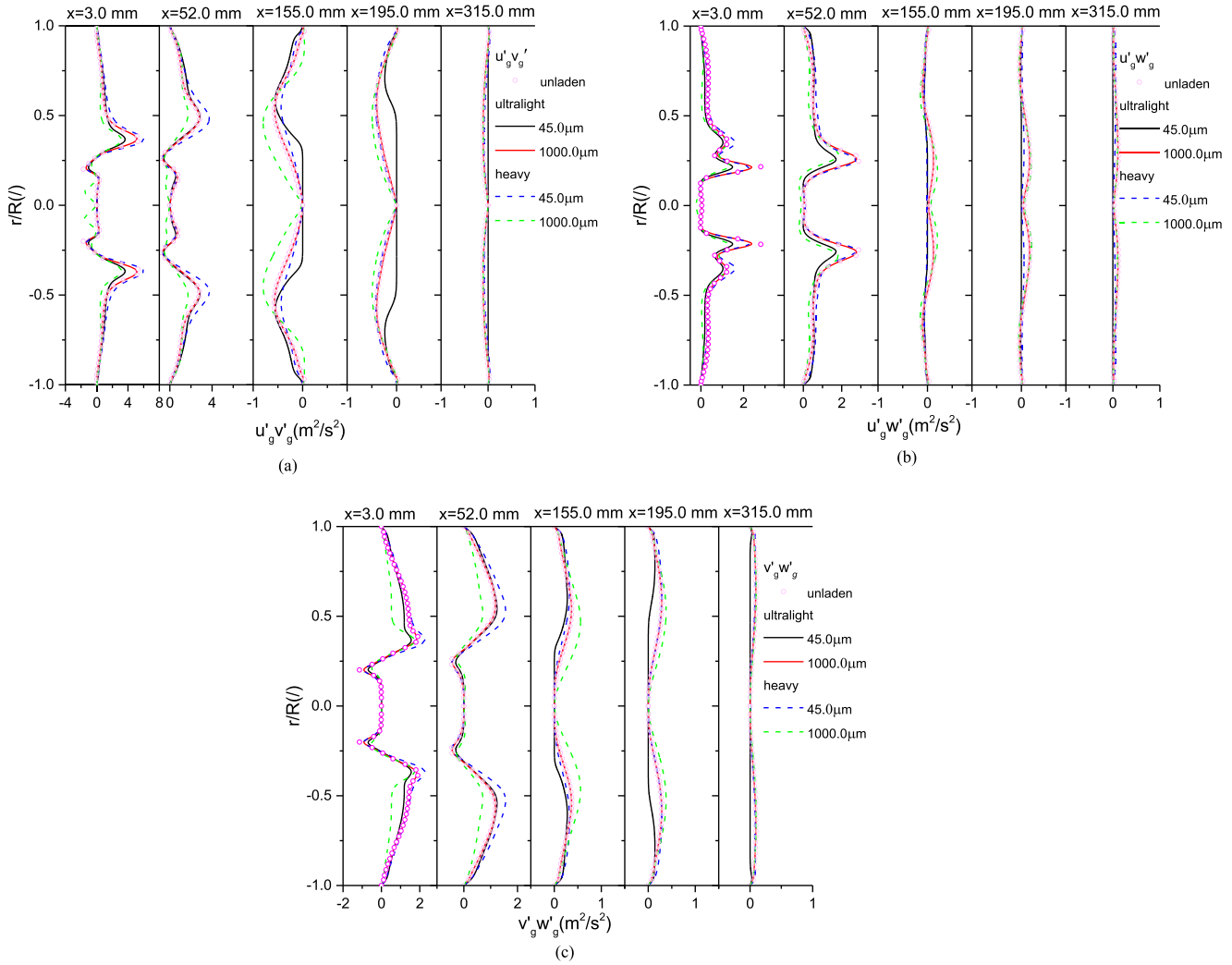

Figure 9. Modulations of gas shear stresses by particles: (a) axial−radial shear stress; (b) axial−tangential shear stress; and (c) radial−tangential shear stress.

fashions. Stokes number is a suitable parameter to judge modulations rather than either diameter or density individuals.

Modulations of Shear Reynolds Stresses by Particles. Figure 9 shows the modulations of the shear Reynolds stress by laden particles. The distributions of shear stresses exhibit significant anisotropic characteristics. Large values located at shear regions due to higher velocity gradients and axial−axial, axial−radial, and radial−tangential values are captured in association with higher values for the axial−axial direction. At the position of x = 50.4 mm and r = 93.0 mm, it reaches up to the maximum and then decreased toward the centerline and the boundary of jet. It is noted that the values at the near inlet region are larger than those of development flows. It can be explained that heavy particles are ready to penetrate the central reversed region; however, light particles are able to quickly response to reversed flow with negative velocity. Overall, modulations of shear stresses are very complicated under the combination effects of centrifugal force, turbulent diffusion, and moment transfer between gas and particle phases. The degrees in axial−radial modulations are stronger than those radial−tangential and axial−tangential directions. The enhancement by the light-small particle and the reduction by the large-heavy particle are acquired because higher preference accumulation concentration is easier to generate at lower vorticity regions. Figure S5 predicted the modulations by heavy particles with St = 1.11 as well as the transition trends in-between larger and smaller Stokes number.

Modulations of the Tensor Invariants of Reynolds Stress by Particles. The tensor invariants of Reynolds stress imply the geometrical and physical information of turbulence fluctuations, which are denoted $I_{g,x}$, $I_{g,y}$, and $I_{g,z}$ using the components of normal and shear Reynolds stress, see eqs T7−T9. Now that invariants indicate the fundamental geometrical and physical characteristics of turbulence fluctuations related with stress components, it is more reasonable to observe the modulations on the invariants than those of any individuals.

$$I_{g,x} = \lambda_{g,x} + \lambda_{g,y} + \lambda_{g,z} = u'_{g,x}u'_{g,x} + u'_{g,y}u'_{g,y} + u'_{g,z}u'_{g,z} \quad (8)$$

$$I_{g,y} = \lambda_{g,x}\lambda_{g,y} + \lambda_{g,x}\lambda_{g,z} + \lambda_{g,z}\lambda_{g,y} = \begin{vmatrix} u'_{g,y}u'_{g,y} & u'_{g,z}u'_{g,y} \\ u'_{g,y}u'_{g,z} & u'_{g,z}u'_{g,z} \end{vmatrix} + \begin{vmatrix} u'_{g,x}u'_{g,x} & u'_{g,z}u'_{g,x} \\ u'_{g,x}u'_{g,z} & u'_{g,z}u'_{g,z} \end{vmatrix} + \begin{vmatrix} u'_{g,x}u'_{g,x} & u'_{g,y}u'_{g,x} \\ u'_{g,y}u'_{g,y} & u'_{g,y}u'_{g,y} \end{vmatrix} \quad (9)$$

https://doi.org/10.1021/acsomega.1c00085
ACS Omega 2021, 6, 10106−10118

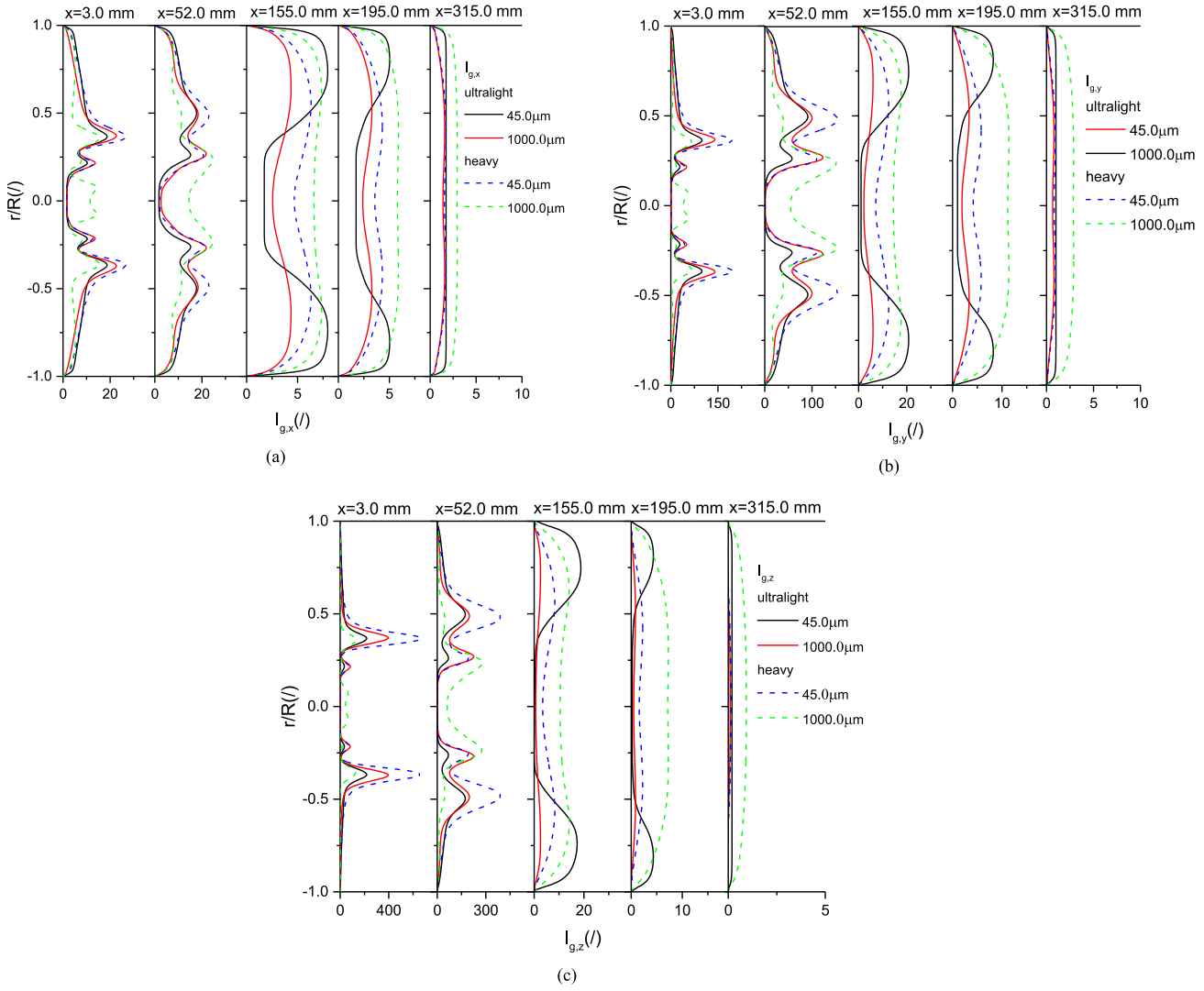

Figure 10. Distributions of stress tensor invariants of gas turbulence: (a) eigenvalues of $I_{g,x}$; (b)eigenvalues of $I_{g,y}$; and (c) eigenvalues of $I_{g,z}$.

$$I_{g,z} = \lambda_{g,x}\lambda_{g,y}\lambda_{g,z} = \begin{vmatrix} u'_{g,x}u'_{g,x} & u'_{g,x}u'_{g,y} & u'_{g,x}u'_{g,z} \\ u'_{g,y}u'_{g,x} & u'_{g,y}u'_{g,y} & u'_{g,y}u'_{g,z} \\ u'_{g,z}u'_{g,x} & u'_{g,z}u'_{g,y} & u'_{g,z}u'_{g,z} \end{vmatrix} \quad (10)$$

Figure 10 shows the modulations of the stress tensor invariants $I_{g,x}$, $I_{g,y}$, and $I_{g,z}$. by particles. Modulations at axial−radial, radial−tangential, and axial−tangential directions are enhanced with an increase in Stokes number. It means that flow structures and vortex rotations were changed by particles although there is same geometry and space configuration.

As mentioned above, larger-heavy particles with large Stokes number have excellent ability to resist the centrifugal force and penetrate the central reserved flow leading to reduction of their dispersions. Turbulent flow structures are quietly complicated, and their mechanism is not clear due to complex multiphase turbulent diffusion, interaction between gas and particle, turbulence scale, Stokes numbers, and so forth. The key parameters related to modulations need to be further validated by experiment.

CONCLUSIONS

In this work, gas turbulence modulations of the swirling gas−particle flow by particles with different diameters and densities were investigated with a large span of Stokes number ranging from 0.0002 to 43.6. The Reynolds stress transport equation to describe the anisotropic characteristics of gas−particle interactions was improved. The particle temperature equation was also coupled to reveal the preferential accumulation at shear stress regions. Modulations of gas turbulence by laden particles indicated the strong anisotropic behaviors, and the mean velocity and fluctuations, Reynolds shear stress, TKE, stress tensor invariants, and vortice structure are quantitatively analyzed. Generally, heavy-large particles with St > 1.0 significantly enhanced the gas turbulence in comparison with that of light-small particles with St < 1.0, except for the axial velocity and axial−radical shear stresses. The anisotropic characteristics caused by preferential accumulations at low vortices are disclosed as well. Further understanding of the mechanism of turbulence modulations and determination of the most dominant factors by a set of parameters of Stokes number, density, diameter, and Reynolds number of particles are still required.

https://doi.org/10.1021/acsomega.1c00085
ACS Omega 2021, 6, 10106−10118

■ ASSOCIATED CONTENT

Supporting Information

The Supporting Information is available free of charge at https://pubs.acs.org/doi/10.1021/acsomega.1c00085.

Simulation results such as the grid independence test and turbulence modulations in-between Stokes number (PDF)

■ AUTHOR INFORMATION

Corresponding Author

Yang Liu − *College of Aerospace Engineering, Taizhou University, Taizhou, Zhejiang 318000, China;* orcid.org/0000-0003-3377-2130; Email: liuya@mail.tsinghua.edu.cn

Authors

Lixiang Jiang − *Beijing Institute of Spacecraft Environmental Engineering, Beijing 10094, China*

Yongju Zhang − *College of Aerospace Engineering, Taizhou University, Taizhou, Zhejiang 318000, China*

Complete contact information is available at: https://pubs.acs.org/10.1021/acsomega.1c00085

Author Contributions

The manuscript was written through the contributions of all authors. All authors have approved the revised version of the manuscript.

Notes

The authors declare no competing financial interest.

■ ACKNOWLEDGMENTS

The authors are grateful for the financial support from the National Science Foundation of China (no. 52078097).

■ NOMENCLATURE

C_D, drag coefficient, (/)
d_s, diameter of the particle, (m)
D, turbophoresis term, (/)
e, restitution coefficient of the particle, (/)
e_w, restitution coefficient of the wall, (/)
g, gravitational acceleration, (m/s^2)
g_0, radial distribution function, (/)
I, unit tensor, (/)
k_g, turbulent kinetic energy of the gas, (m^2/s^2)
k_s, turbulent kinetic energy of the particle, (m^2/s^2)
p, thermodynamic pressure, (Pa)
p_p, particle phase pressure, (Pa)
pfp, particle frictional pressure, (Pa)
P, production term, (/)
$\dot{m}$, mass flow rate, (g/s)
Re_s, particle Reynolds number, (/)
s, swirling number, (/)
St, Stokes number, (/)
t, time, (s)
T, interaction term, (/)
u_g, gas velocity, (m/s)
u_s, particle velocity, (m/s)

■ GREEK ALPHABETS

α_g gas volume fraction, (/)
α_s particle volume fraction, (/)
$\alpha_{s,max}$ maximum particle volume fraction, (/)
β_{gs} inter-phase drag coefficient, (/)
γ collisional dissipation rate, (kg/ms^3)
λ eigenvalues of the tensor, (/)
δ kronic-delta unit tensor, (/)
ρ_g gas density, (kg/m^3)
ρ_s particle density, (kg/m^3)
ε_g turbulent energy dissipation rate of the gas, (m^2/s^3)
ε_s turbulent energy dissipation rate of the particle, (m^2/s^3)
η particle mass loading, (/)
μ_g gas dynamic viscosity, (Pa·s)
μ_s particle shear viscosity, (Pa·s)
τ_g stress tensor of the gas phase, (Pa)
τ_p stress tensor of the particle phase, (Pa)
ξ_s particle bulk viscosity, (Pa·s)
θ particle temperature, (m^2/s^2)
Π pressure−strain, (/)
τ_s particle relaxation time, (s)
τ_f fluid time scale, (s)
φ particle sphericity (/)
ϕ blending function, (/)

■ SUPERSCRIPTS

’ fluctuation
– averaged

■ SUBSCRIPTS

an annular
i,j,k coordinates’ directions
in inlet
f frictional flow
g,s gas and particle
l laminar
L length
o outer
r relax

■ REFERENCES

(1) Gupta, A.; Lilley, D. G.; Syred, N. *Swirl Flows*; Abacus Press: Tunbridge Wells, 1984; pp 32−67.

(2) Gidaspow, D. *Multiphase Flow and Fluidization: Continuum and Kinetic Theory Description*; Academic Press: New York, 1994; pp 45−60.

(3) Crowe, C.; Sommerfeld, M. S.; Tsuji, Y. *Multiphase Flows with Droplets and Particles*; CRC Press: Boca Raton, 1998; pp 67−88.

(4) Liu, Y.; Zhang, L.; Chen, Z.; Zhou, L. Numerical investigation on mixture particle dispersion characteristics in swirling particle-laden combustion chamber. *Int. Commun. Heat Mass Tran.* **2020**, *117*, 104720.

(5) Liu, Y.; Chen, Z.; Zhang, Y.; Zhou, L. Hydrodynamic modeling of swirling binary mixture gasp-article flows using a second order moment turbulence model. *ACS Omega* **2020**, *5*, 31490−31501.

(6) Yoon, J. S.; Yoon, Y. Y. Comparative study of mixing characteristics of particle-laden shear and swirl coaxial jets. *J. Propul. Power* **2017**, *33*, 1−9.

(7) Kulick, J. D.; Fessler, J. R.; Eaton, J. K. Particle response and turbulence modification in fully developed channel flow. *J. Fluid Mech.* **1994**, *277*, 109−134.

(8) Fessler, J. R.; Eaton, J. K. Turbulence modification by particles in a backward-facing step flow. *J. Fluid Mech.* **1999**, *394*, 97−117.

(9) Ljus, C.; Johansson, B.; Almstedt, A.-E. Turbulence modification by particles in a horizontal pipe flow. *Int. J. Multiphase Flow* **2002**, *28*, 1075−1090.

(10) Mora, D. O.; Cartellier, A.; Obligado, M. Experimental estimation of turbulence modification by inertial particles at moderate Re_λ. *Phys. Rev. Fluids.* **2019**, *4*, 074309.

(11) Kiger, K. T.; Pan, C. Suspension and turbulence modification effects of solid particulates on a horizontal turbulent channel flow. *J. Turbul.* **2002**, *3*, 1−21.
(12) Wu, Y.; Wang, H.; Liu, Z.; Li, J.; Zhang, L.; Zheng, C. Experimental investigation on turbulence modification in a horizontal channel flow at relatively low mass loading. *Acta Mech. Sin.* **2006**, *22*, 99−108.
(13) Sommerfeld, M.; Qiu, H.-H. Detailed measurements in a swirling particulate two-phase flow by a phase Doppler anemometer. *Int. J. Heat Fluid Flow* **1991**, *12*, 20−28.
(14) Sommerfeld, M.; Qiu, H.-H. Characterization of particle-laden, confined swirling flows by a phase-doppler anemometer. *Int. J. Heat Fluid Flow* **1993**, *19*, 1093−1127.
(15) Al-Abdeli, Y. M.; Masri, A. R. Review of laboratory swirl burners and experiments for model validation. *Exp. Therm. Fluid Sci.* **2015**, *69*, 178−196.
(16) Fang, C. C.; Xu, J. L.; Liu, H. F. Influences of the cross angle on the dispersion characteristics in a dense gas-particle coaxial jet. *Ind. Eng. Chem. Res.* **2016**, *55*, 11160−11166.
(17) Rajamanickam, K.; Basu, S. On the dynamics of vortex-droplet interactions, dispersion and breakup in a coaxial swirling flow. *J. Fluid Eng.* **2017**, *827*, 572−613.
(18) Cabeza, C.; Sarasúa, G.; Martí, A. C.; Bove, I.; Varela, S.; Usera, G.; Vernet, A. Influence of coaxial cylinders on the vortex breakdown in a closed flow. *Eur. J. Mech. B Fluid* **2010**, *29*, 201−207.
(19) Eaton, J. K. Experiments and simulations on turbulence modification by dispersed particles. *Appl. Mech. Rev.* **1994**, *47*, S44−S48.
(20) Gui, N.; Fan, J. R.; Chen, S. Numerical study of particle-vortex interaction and turbulence modulation in swirling jets. *Phys. Rev. E—Stat. Nonlinear Soft Matter Phys.* **2010**, *82*, 056323.
(21) Yan, J.; Gui, N.; Xie, G.; Gao, J. Direct numerical simulation of particle-laden swirling flows on turbulence modulation. *Math. Probl. Eng.* **2014**, *2014*, 1−12.
(22) Yan, J.; Gui, N.; Xie, G.; Gao, J. Direct numerical simulation and visualization of biswirling jets. *Math. Probl. Eng.* **2014**, *6*, 193731.
(23) Wang, G.; Richter, D. H. Modulation of the turbulence regeneration cycle by inertial particles in planar Couette flow. *J. Fluid Mech.* **2019**, *861*, 901−929.
(24) Wang, B.; Zhang, H. Q.; Wang, X. L. Large eddy simulation of particle-laden turbulent flows over a backward-facing step considering two-phase two-way coupling. *Adv. Mech. Eng.* **2013**, *325*, 325101.
(25) Apte, S. V.; Mahesh, K.; Moin, P.; Oefelein, J. C. Large-eddy simulation of swirling particle-laden flows in a coaxial-jet combustor. *Int. J. Multiphase Flow* **2003**, *29*, 1311−1331.
(26) Joseph, C.; Oefelein, V.; Drozda, G. Large eddy simulation of swirling particle laden flow in model axisymmetric combustor. *Proc. Combust. Inst.* **2007**, *31*, 2291−3229.
(27) Brauner, T.; Jones, W. P.; Marquis, A. J. LES of the cambridge stratified swirl burner using a sub-grid pdf approach. *Flow, Turbul. Combust.* **2016**, *96*, 965−985.
(28) Liu, Y.; Zhou, L. X.; Xu, C. X. Numerical simulation of instantaneous flow structure of swirling, and non-swirling coaxial jet particle laden turbulence flows. *Phys. Stat. Mech. Appl.* **2010**, *389*, 5380−5389.
(29) Liu, Y.; Lu, H. L.; Liu, W. T. Model and simulation of gas-solid flow with wide size distributions in circulating fluidized bed. *J. Ind. Eng. Chem.* **2003**, *54*, 106−1071.
(30) Syred, N. A review of oscillation mechanisms and the role of the processing vortex core (PVC) in swirl combustion systems. *Prog. Energy Combust. Sci.* **2006**, *32*, 93−161.
(31) Elghobashi, S. Direct numerical simulation of turbulent flows laden with droplets or bubbles. *Annu. Rev. Fluid Mech.* **2019**, *51*, 217−244.
(32) Anagnostopoulos, J. S.; Bergeles, G. C. Discrete-phase effects on the flow field of a droplet-laden swirling jet with recirculation: a numerical study. *Int. J. Heat Fluid Flow* **1992**, *13*, 141−150.
(33) Sommerfeld, M.; Ando, A.; Wennerberg, D. Swirling, particle-laden flows through a pipe expansion. *J. Fluid Eng.* **1992**, *114*, 648−656.
(34) Zhang, Y.; Reese, J. M. Gas turbulence modulation in a two-fluid model for gas-solid flows. *AIChE J.* **2003**, *49*, 3048−3065.
(35) Tanaka, T.; Eaton, J. K. Classification of turbulence modification by dispersed spheres using a novel dimensionless number. *Phys. Rev. Lett.* **2008**, *101*, 114502.
(36) Pakhomov, M. A.; Terekhov, V. I. Numerical simulation of turbulent swirling gas-dispersed flow behind a sudden tube expansion. *Thermophys. Aeromechanics* **2015**, *22*, 597−608.
(37) Lin, J.; Shen, S. Numerical simulation of turbulence modulation by cylindrical particles in round jet. *Eng. Appl. Comp. Fluid Mech.* **2014**, *8*, 345−355.
(38) Zhou, L. Two-fluid turbulence modeling of swirling gas-particle flows-A review. *Powder Technol.* **2017**, *314*, 253−263.
(39) Liu, Y.; Zhang, Y.; Zhou, L. Numerical study on bubble-liquid two-phase turbulent hydrodynamics in extremely narrow shape bioreactor. *Int. Commun. Heat Mass Tran.* **2019**, *108*, 104286.
(40) Liu, Y.; Zhang, L.; Zhou, L. Effects of swirling flow on ultralight-particle dispersion characteristics in coaxial jet combustor. *Energy Sci. Eng.* **2019**, *7*, 3220−3233.
(41) Liu, Y.; Zhou, L.; Zhang, Y. Numerical Simulation of bubbles-liquid two-phase turbulent in shallow bioreactor. *Energies* **2019**, *12*, 2269−2282.
(42) Liu, Y.; Zhang, L.; Zhou, L. Development of modeling and simulation of bubble liquid hydrodynamics in bubble column. *Energy Sci. Eng.* **2020**, *8*, 327−339.
(43) Liu, Y.; Zhang, L.; Zhang, Y.; Zhou, L. Effects of sparger holes on gas-liquid hydrodynamics in bubble column. *Chem. Eng. Technol.* **2020**, *43*, 307−316.
(44) Johnson, P. C.; Nott, P.; Jackson, R. Frictional-collisional equations of motion for participate flows and their application to chutes. *J. Fluid Mech.* **1990**, *210*, 501−535.
(45) Gore, R. A.; Crowe, C. T. Effect of particle size on modulation in turbulent intensity. *Int. J. Multiphase Flow* **1989**, *15*, 279−285.
(46) Elghobashi, S. On predicting particle-laden turbulent flows. *Appl. Sci. Res.* **1994**, *52*, 309−329.

https://doi.org/10.1021/acsomega.1c00085
ACS Omega 2021, 6, 10106−10118